Research Article Vol. 29, No. 24 / 22 Nov 2021 / Optics Express 39449
Optics EXPRESS

Frequency-based dispersion Lamb-dip spectroscopy in a high finesse optical cavity

KATARZYNA BIELSKA,* AGATA CYGAN, MAGDALENA KONEFAŁ, GRZEGORZ KOWZAN, MIKOŁAJ ZABOROWSKI, DOMINIK CHARCZUN, SZYMON WÓJTEWICZ, PIOTR WCISŁO, PIOTR MASŁOWSKI, ROMAN CIURYŁO, AND DANIEL LISAK

Institute of Physics, Faculty of Physics, Astronomy and Informatics, Nicolaus Copernicus University in Toruń, Grudziadzka 5, 87-100 Toruń, Poland
*kbielska@umk.pl

Abstract: Frequency-based cavity mode-dispersion spectroscopy (CMDS), previously applied for Doppler-limited molecular spectroscopy, is now employed for the first time for saturation spectroscopy. Comparison with two intensity-based, cavity-enhanced absorption spectroscopy techniques, i.e. cavity mode-width spectroscopy (CMWS) and the well-established cavity ring-down spectroscopy (CRDS), shows the predominance of the CMDS. The method enables measurements in broader pressure range and shows high immunity of the Lamb dip position to the incomplete model of saturated cavity mode shape. Frequencies of transitions from the second overtone of CO are determined with standard uncertainty below 500 Hz which corresponds to relative uncertainty below 3×10^{-12}. The pressure shift of the Lamb dips, which has not been detected for these transitions in available literature data, is observed.

© 2021 Optical Society of America under the terms of the OSA Open Access Publishing Agreement

1. Introduction

Accurate spectroscopy of atoms and molecules is a basic tool for tests of fundamental physics [1] not only in the simplest molecular systems but also with polyatomic molecules [2]. Such fundamental research based on atomic and molecular systems has multiple applications in subjects such as quantum electrodynamics (QED) tests [3–5], determination of physical constants and their variability [6,7], measurements of the electric dipole moment of electron and the electron shape [8,9], searching for new forces [3,10] and the dark matter [11,12]. Accurately known molecular transition frequencies can also serve as frequency standards [13].

In the above-mentioned applications and many others, the molecular transition frequencies need to be measured with unprecedented accuracy. The most common measurements of Doppler-broadened transitions typically attain megahertz or sub-megahertz accuracy. Kilohertz accuracy has already been achieved [14–16]. Recently, CO_2 transition frequencies from the (30012) ← (00001) band were determined with minimum combined uncertainty of 200 Hz [17]. In the Doppler regime such low measurement uncertainties are possible only for well isolated transitions. On the other hand, kHz uncertainties and lower are typical for Doppler-free techniques, such as saturation spectroscopy, that make it possible to resolve and accurately determine frequencies of transitions separated by less than the Doppler width [18].

Many molecular transitions in the visible and near-infrared range have relatively low intensities. This prevents not only saturation spectroscopy measurements but also standard absorptive measurements from being performed with sufficient signal-to-noise ratio in a single-pass absorption cell. A high-finesse optical cavity can be used both to enhance the absorption path length and to induce saturation conditions by enhancing optical power in the system. Saturation spectroscopy has already been applied in multiple techniques based on optical cavities. Apart from simple cavity-enhanced spectroscopy (CEAS) [19], it has been demonstrated and successfully

#443661 https://doi.org/10.1364/OE.443661
Journal © 2021 Received 19 Sep 2021; revised 27 Oct 2021; accepted 27 Oct 2021; published 10 Nov 2021

Optics EXPRESS

used in techniques such as cavity ring-down spectroscopy (CRDS) [20,21] and noise-immune cavity-enhanced optical heterodyne molecular spectroscopy (NICE-OHMS) [22,23].

In this work, we apply for the first time the cavity mode-dispersion spectroscopy (CMDS) [24] and cavity mode-width spectroscopy (CMWS) [25,26] techniques in saturation conditions. CMDS is a recently developed one-dimensional, frequency-based spectroscopic technique that relies on determination of dispersive shifts of high-finesse cavity modes. In a Doppler-limited non-saturated spectroscopy technique, CMDS offers significantly wider dynamic range and higher accuracy than the absorption-based CEAS, CRDS and CMWS techniques [27]. In the last two cases, the absorption coefficient is determined from measurements of the photon life time in the cavity and of the cavity mode width, respectively. One of the main limitations of CRDS is related to the non-linearity of the detection system [28]. This problem can be overcome by proper calibration of the detection system [29]. On the other hand, CMDS enables similar accuracy without the necessity of such calibration procedures [27]. In contrast to CRDS and CMWS, a CMDS spectrum is determined from central frequencies of cavity modes and not from the light intensity or its dependence on time. The CMDS, CMWS, and CRDS techniques can be implemented in the same experimental setup both for Doppler-limited and saturation spectroscopy. In the present work, applicability of all those techniques to saturation spectroscopy is compared and carefully analyzed. We apply the sub-Doppler CMDS technique to measurements of transitions from the second overtone ((3 $\leftarrow$ 0) band) of the CO molecule in the spectral range near 1.57 μm.

2. Experimental details

2.1. Experimental setup

The measurements are performed with the spectrometer described in Ref. [27], which is slightly modified for the purpose of the present study. The high-finesse optical cavity is 73-cm long and consists of two spherical mirrors in non-confocal configuration. The intensity reflectivity of the mirrors at the wavelength of CO transitions (1.57 μm) reaches $R \approx 0.999992$ and at the wavelength of the Nd:YAG laser (1.064 μm) it reaches $R \approx 0.98$. The finesse of the cavity filled with a non-absorptive sample is $\mathcal{F} \approx 390\,000$ at 1.57 μm, corresponding to the full width at half maximum (FWHM) of the cavity mode of $\delta\nu \approx 0.54$ kHz and the ring-down time decay constant of $\tau \approx 300$ μs. The increased reflectivity of the mirrors and thus the higher finesse is the main difference between the present and previous arrangement of the spectrometer. It enables higher intra-cavity probe beam power, which in our measurements is up to 170 W for the coupling efficiency of approximately 20%. The cavity length is actively stabilized [30] in reference to the frequency of the I_2-stabilized Nd:YAG laser, which prevents drifts due to variations in laboratory pressure and temperature. One of cavity mirrors is mounted on a piezo transducer and can be moved along the cavity optical axis in a controlled way. It enables shifting positions of the cavity modes in the frequency domain and thus spectra acquisition with frequency step lower than the cavity free spectral range (FSR), which is approximately 204.5 MHz. The cavity temperature is actively stabilized at 296 K within ±50 mK. As a probe gas we use a commercial sample of CO with 0.99997 purity. The sample pressure in the cavity is determined from Doppler-limited measurements before and after the Lamb dip measurement and referenced to HITRAN [31] line intensities with uncertainty below 2%.

The probe laser is an external-cavity diode laser (ECDL) which emits in the spectral range near 1.57 μm. The system is arranged in a dual-beam configuration [27,32,33]. Part of the laser beam is used as a locking beam for locking the laser frequency to the cavity resonance with the Pound-Drever-Hall technique (PDH) [34], which also enables beam spectral narrowing [35]. Based on our previous studies [36], we estimate the spectral width of the laser relative to the cavity mode frequency to be below 40 Hz. The bandwidth of the PDH lock servo loop is above 1 MHz. Another part of the beam, with polarization orthogonal to the locking one, serves as the

Optics EXPRESS

actual probe beam and is phase-modulated with an electro-optic modulator (EOM) working in the frequency range from 200 MHz to 20 GHz, amplified with booster optical amplifier (BOA) and frequency-shifted with an acousto-optic modulator (AOM). This configuration enables the use of a first-order EOM side-band as the probe beam. The AOM triggers ring-down decays for the CRDS and ensures that neither the carrier frequency nor EOM side-bands, other than the selected positive or negative first-order one, are in resonance with the cavity. The orthogonality of probe and locking beam polarizations enables their separation behind the cavity. For this purpose a polarizing beam splitter with extinction ratio of 1000:1 is used. Part of the laser beam is also used to generate a beat-note signal between the laser and an optical frequency comb (OFC), which enables determination of the probe beam absolute frequency at each spectral point, based on the OFC offset frequency ($f_0 \approx 20$ MHz), repetition rate ($f_{\mathrm{rep}} \approx 250$ MHz), beat-note frequency and frequencies of RF signals driving the EOM and AOM. A wavemeter of accuracy better than $f_{\mathrm{rep}}/2$ is used to determine the number of the comb tooth nearest to the laser frequency. The signal generators driving the EOM and AOM, frequency counters and the OFC are referenced to the stable 10 MHz RF signal (stability of 10^{-12} at 1 s) delivered to our laboratory from the Astro-Geodynamic Observatory in Borowiec, Poland by a fiber link [36].

2.2. CRDS, CMWS and CMDS in saturation conditions

The CRDS technique has already been applied to measurements in saturation conditions in different laboratories. In the Doppler regime, CRDS relies on determination of the time constant, τ, of the exponential decay of light intensity, I, at the ring-down cavity output: $I(t) = I_0 \exp(-t/\tau)$. The absorption coefficient, α, is then determined as $\alpha = 1/(c\tau) - \alpha_{\mathrm{bg}}$, where α_{bg} corresponds to the cavity base losses and c is the speed of light. In saturation conditions as the intracavity power decreases, the absorption coefficient increases, which leads to non-exponential ring-down decay signals [18,20,37]. However, in a typical approach designed to measure Lamb dip positions, it is assumed that the saturation is weak and a single-exponential decay is fitted [38,39]. As a consequence, the derived absorption coefficient has an intermediate value between saturated and non-saturated absorption. An example of such saturated ring-down decay together with the residuals from the fit of an exponential function is shown in Fig. 1 in panels (e) and (f), respectively. In this approach the Lamb dip position is determined but its shape cannot be accurately derived.

In CMWS, the absorption coefficient is derived from the full width at half maximum (FWHM) of the cavity mode, $\delta\nu$, and from the refractive index of the sample, n: $\alpha = 2\pi n\delta\nu/c - \alpha_{\mathrm{bg}}$ [25]. In the CMDS technique, from the same measurement of the cavity mode shape its position in the frequency domain is derived. The difference, $\Delta\nu_D$, between the measured mode position and its position resulting from linear dependence of the longitudinal mode order versus frequency, is the measure of the resonant sample dispersion. This linear dependence arises from the cavity length and broadband dispersion which in the limited spectral range can be approximated as constant.

In contrast to a Doppler-broadened line, a Lamb dip is a narrow spectral feature. In our conditions its width is more than two orders of magnitude below the cavity FSR. To probe it, it is necessary to reduce the spectrum frequency step much below the cavity FSR, which is done by controlled changes of the cavity length, thus scanning the resonant frequency of selected cavity mode (probe mode) across the Lamb dip. In such case the corresponding change of the cavity FSR needs to be accounted for [24], as explained below.

In our approach to CMDS the reference cavity FSR, ν_{FSR0}, is determined before the scan across the Lamb dip by measuring frequencies of two cavity modes far from the resonant dispersion. The laser is frequency-locked to the N-th order cavity mode (lock mode) at central frequency ν_{l0} far from the resonant dispersion, see Fig. 2, whereas the probe mode of order $N + k$ at central frequency $\nu_{p0} = \nu_{l0} + k\nu_{\mathrm{FSR0}} + \Delta\nu_{D0}$ is measured. If ν_{FSR0} changes by $\Delta\nu_{\mathrm{FSR}}$ due to change of the cavity length, positions of the lock and probe modes shift to $\nu_l = \nu_{l0} + N\Delta\nu_{\mathrm{FSR}}$

Optics EXPRESS

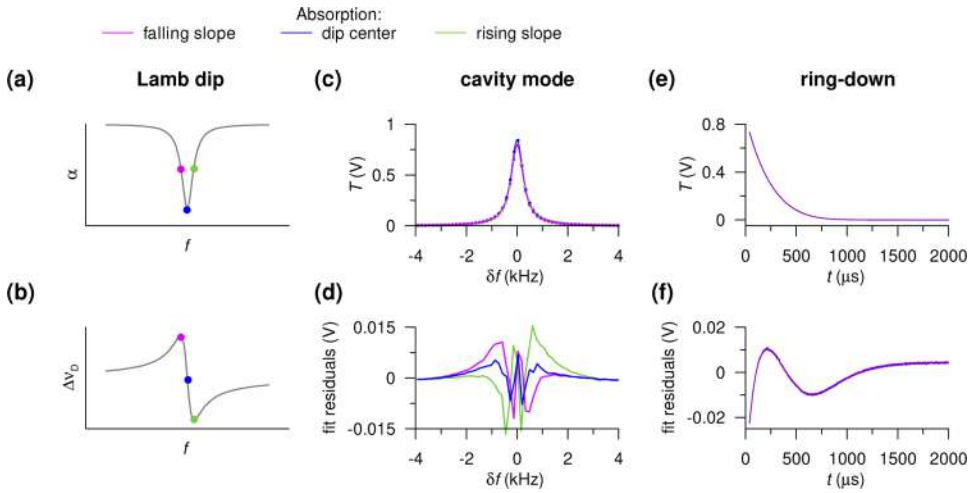

Fig. 1. Signals in CRDS, CMDS and CMWS in saturation conditions. (a) Simulations of an absorptive and (b) dispersive Lamb dip. The three points marked in color correspond to the dip center, its falling and rising absorptive slope. (c) Measured transmission, T, through the cavity mode as function of the detuning from the cavity mode center, δf, corresponding to the three spectral points marked out in panels (a) and (b). (d) Residuals from the fit of Lorentzian function to the measured cavity mode shape for the three spectral points. (e) Saturated ring-down decay and (f) residuals from the fit of single-exponential decay. The decay is fitted with a function $y = a\exp(-t/\tau) + b$, where τ is the fitted time decay constant, t is time, a is the decay amplitude, and b accounts for possible offsets in electrical signals.

and $\nu_p = \nu_l + k\,(\nu_{\mathrm{FSR}0} + \Delta\nu_{\mathrm{FSR}}) + \Delta\nu_D$, respectively. Frequencies $\Delta\nu_{D0}$ and $\Delta\nu_D$ are the relevant mode shifts due to resonant dispersion at two considered points of the measured spectrum. Frequencies ν_{l0}, ν_l and mode order N are determined from measurements of the locking beam optical frequency with the OFC, whereas $(\nu_{p0} - \nu_{l0})$ and $(\nu_p - \nu_l)$ are determined from the mode center fits and the change of cavity FSR is calculated as $\Delta\nu_{\mathrm{FSR}} = \nu_{\mathrm{FSR}0}\,(\nu_l - \nu_{l0})\,/\nu_{l0}$.

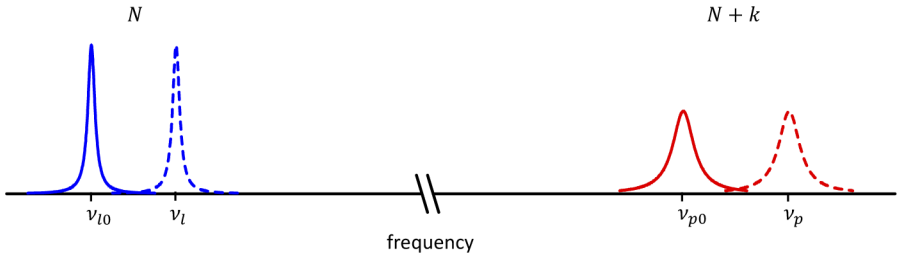

Fig. 2. Lock (blue) and probe (red) cavity mode in presence of resonant dispersion in the region of the probe mode. Solid lines indicate cavity modes and their positions on the frequency axis for given cavity length, whereas dashed lines show cavity modes of the same orders after changing the cavity length and thus the FSR. Note that the probe mode shifted due to the resonant dispersion is also broadened due to associated resonant absorption.

In saturation-free case, the cavity mode shape can be approximated with a Lorentzian function. Similarly to CRDS, the CMWS and CMDS techniques can be implemented in saturation conditions. Following the standard approach to CRDS in saturation conditions, in CMWS and CMDS we assume non-saturated mode shape and determine the cavity mode width and its central frequency from the fit of a Lorentzian function. In panel (c) of Fig. 1, measured cavity modes

Optics EXPRESS

in saturation conditions are presented as functions of the detuning from the mode center, δf. Panel (d) presents residuals from the fit of a Lorentzian function to the measured cavity mode for the three spectral points marked in panels (a) and (b). The cavity mode shape is clearly non-Lorentzian due to saturation and the reason is similar as in the case of non-exponential ring-down decay: for different detunings from the mode center, the intra-cavity power is different, which leads to different values of the saturation parameter and thus of the absorption coefficient. Fit residuals corresponding to the point located near the Lamb dip center are symmetric. In contrast, fit residuals corresponding to spectral points detuned from the Lamb dip center towards lower and higher frequencies, are not only non-Lorentzian but also non-symmetric with opposite asymmetries. Their asymmetry is caused by the fact that on the absorption slope of a narrow Lamb dip, the absorption coefficient is changing across the cavity mode. Due to saturation, this effect is enhanced. Cavity mode shapes in the present study are fitted with a symmetric Lorentzian function beacuse at present there is no analytical model of saturated mode shape available. This causes that similarly as in CRDS, only the Lamb dip position can be accurately determined, whereas conclusions on the dip shape cannot be reliably made [37].

The choice of time interval for fitting the decay in CRDS or frequency detuning range for the mode shape fitting in the CMDS and CMWS techniques may significantly affect the determined Lamb dip position in the absorptive techniques. In the measurement procedure, immediately after recording ring-down decays, cavity mode shape was measured at each spectral point. In Fig. 3 there are presented Lamb dip positions obtained with these three spectroscopic techniques,

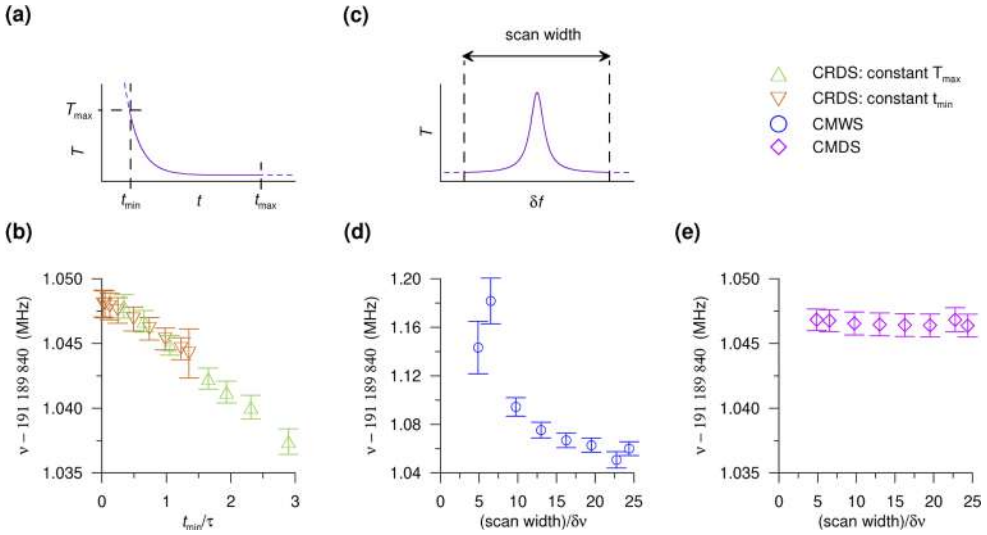

Fig. 3. Determined position of the lamb dip, ν, measured for the R7 transition from the second overtone band of CO molecule at pressure of 0.5 Pa, vs cavity ring down or cavity mode shape fitting range. (a) Ring-down decay and two approaches to the choice of its fitting range: either each decay is cut at the same signal level $T_{\max}$ (green triangles in panel (b)) or decay fit starts after delay $t_{\min}$ from turning off the probe beam (orange triangles in panel (b)). (b) The Lamb dip position resulting from CRDS measurements vs initial part of the decay excluded from the fit as explained in panel (a). Time axis is in units of decay time constant, τ, for the decay corresponding to the Lamb dip center. (c) The cavity mode shape as a function of detuning from the mode center, δf, and the fitted scan range, symmetric with respect to the mode center. (d) The Lamb dip position resulting from CMWS and (e) CMDS measurements vs the cavity mode shape fitting range expressed in units of the maximal measured cavity mode width, $\delta\nu$.

Optics EXPRESS

based on a measurement performed for the R7 transition at pressure of 0.5 Pa. In order to validate the retrieved Lamb dip positions, acquired signals were fitted for different ring-down decay acquisition times and cavity mode scan widths as shown in panels (a) and (c). In panel (b) the Lamb dip position is plotted versus the length of the initial part of the ring-down decay that was excluded from the fit, for the spectral point corresponding to the Lamb dip center. Different parts of the recorded decay are removed from its beginning, leading to the dip position varying by approximately 11 kHz, with the position uncertainty close to 1 kHz. Panel (d) shows the dependence of the determined Lamb dip position on the width of scan around the cavity mode which is used for fitting its shape. This position varies by 130 kHz for the fitting range varying by a factor of 4. Panel (e) shows dip positions obtained from the same data as CMWS ones but interpreted in terms of CMDS. For the fitted scan range varying within the same limits as for CMWS it leads to the dip position which remains constant within sub-kHz uncertainty. Based on this comparison, in our experimental setup only CMDS technique enables reliable determination of the Lamb dip position. An advantage of a dispersive Lamb-dip spectrum is the immunity of the Doppler-broadened envelope profile to the saturation effect, as shown in Ref. [40]. As a result, variation in the laser power should cause asymmetry of the Doppler envelope and thus distortion (asymmetry) of the absorptive Lamb dip, which leads to the shift of fitted position, but not of the dispersive one. The magnitude of this shift depends on the decay or mode

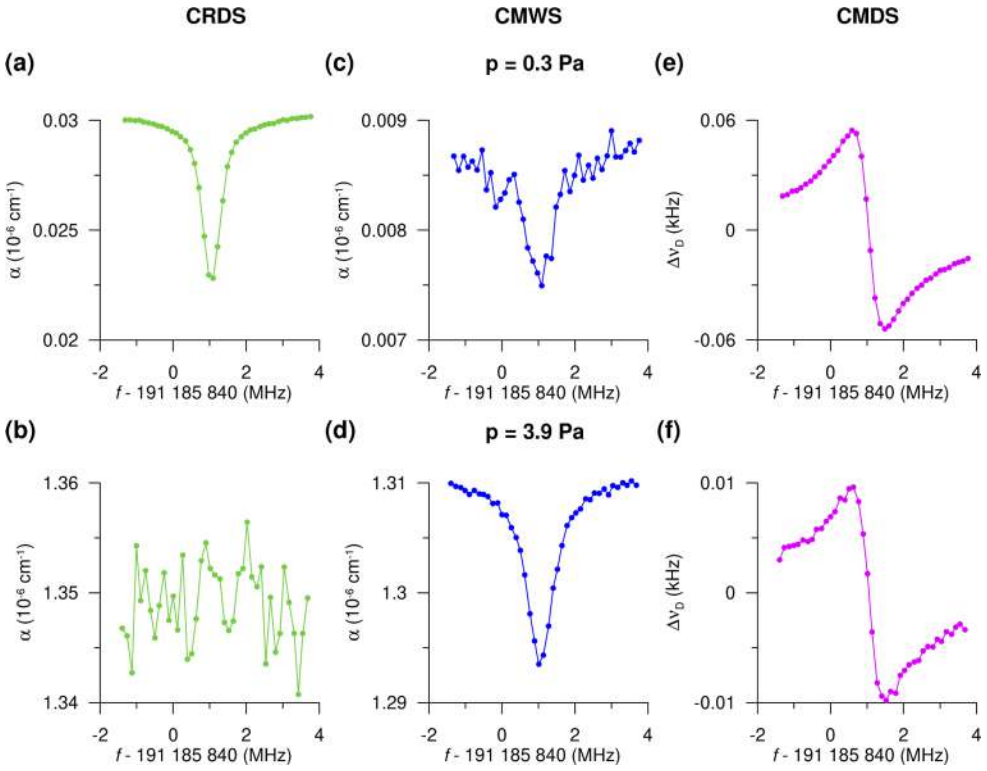

Fig. 4. Dispersive and absorptive Lamb dip measured for R7 transition from the second overtone band of CO molecule for two sample pressures: 0.3 Pa (top row) and 3.9 Pa (bottom row) with three experimental techniques: CRDS (panels (a) and (b)), CMWS (panels (c) and (d)) and CMDS (panels (e) and (f)). In CRDS measurements shown here, the ring-down decay fitting range starts after cutting off not more than 1.3τ. In CMWS and CMDS the cavity mode width fitting range equals at least $15\delta\nu$.

Optics EXPRESS

shape fitting range, as shown in Fig. 3(b) and (d). In general, the determination of the Lamb dip central frequency can also be affected by the change in cavity mirror properties caused by heating them up with the probe beam. We have observed this effect in our recent work performed on a different experimental setup in the spectral range near 0.69 μm [41]. If cavity mirrors change their properties during the measurement, especially the reflectivity, the measured absorptive dip becomes asymmetric again.

The three measurement techniques have different signal-to-noise ratio (SNR) of the Lamb dip in the same conditions, i.e. for the same transition, pressure and available optical power. Lamb dips recorded with CRDS, CMWS and CMDS in the same experimental conditions, for two different sample pressures, are shown in Fig. 4. CRDS measurements lead to clearly outlined absorption Lamb dip in a low pressure range (panel (a)), however it is invisible in case of higher pressure (panel (b)). In case of the CMWS spectra it is the opposite: the dip is barely visible in the case of low pressure (panel (c)) and it is clearly outlined in higher pressure (panel (d)). Also, significantly different absorption levels in CRDS and CMWS indicate the effect of fitting the exponential decay and Lorentzian shape of the cavity mode, none of which properly accounts for saturation. In contrast to that, CMDS enables saturation measurements in the broadest range of measurement conditions and leads to clear dispersive Lamb dip both in lower and higher sample pressure (panels (e) and (f)). This conclusion follows the one made for Doppler-limited spectroscopy in saturation-free conditions, where we have shown that it is the most accurate technique among these three in the widest dynamic range [27].

3. Measurements and results

Two transitions from the second overtone band of CO, namely R7 and R10, were measured with the CMDS technique in the pressure range from 0.3 Pa to 4 Pa. Determined Lamb dip positions plotted against sample pressure are shown in Fig. 5. The amplitude ratio of the Lamb dip to the Doppler-broadened line shape varies from 0.3 in the lowest pressure to 0.004 in the highest pressure. The Lamb dip shape is fitted with the dispersive Lorentzian function and SNR up to 370. Based on weighted linear regression to the dip positions measured in the range of pressures, we determine transition frequencies as well as the collisional shift coefficients in saturation conditions. Those results are given in Table 1 together with the literature values.

Table 1. Determined transition frequencies extrapolated to zero pressure, ν_0, collisional shift coefficients, Δ/p, and comparison with literature values.

transition	ν_0 (kHz)	Δ/p (kHz/Pa)
This work		
R7	191 189 841 046.10(38)	−1.05(33)
R10	191 440 612 667.66(48)	−1.16(32)
Wang et al. [39,42,43]		
R7	191 189 841 045.4(8)	
R10	191 440 612 665.1(5)	
Mondelain et al. [44]		
R7	191 189 840 950(300)	
R10	191 440 612 430(300)	
Picqué et al. [45]		
R7	191 189 840 400(900)	−1.8(3)
R10	191 440 611 900(900)	−1.8(3)

Table 2 gives the uncertainty budget for transition R7. As the frequency reference we use an RF signal (10 MHz) of relative stability during 1 s at 10^{-12} level, which at the frequency of transitions

Optics EXPRESS

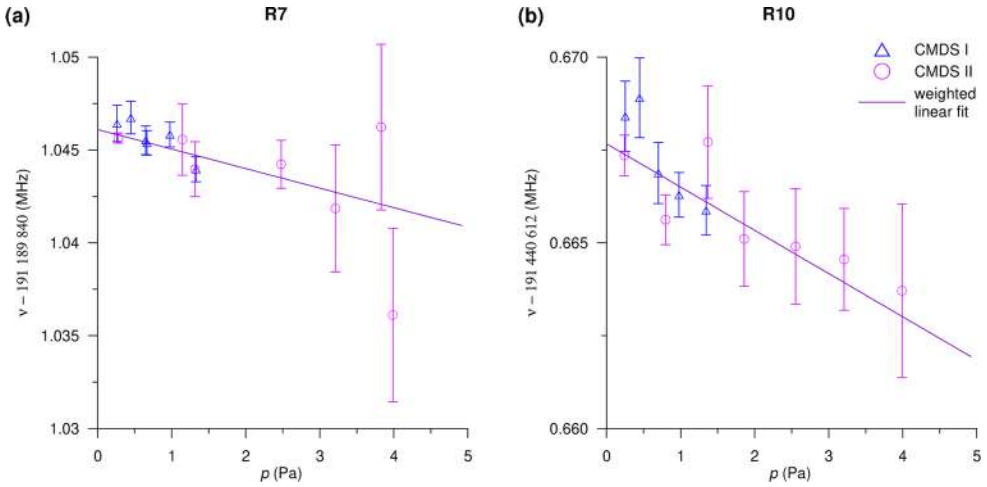

Fig. 5. Position of R7 (panel (a)) and R10 (panel (b)) transitions from the second overtone of CO, measured in the saturation regime with the CMDS technique, against sample pressure, p. Triangles (△) and circles (○) indicate two measurement series performed with two independent OFCs, within the time span of two years. Solid lines show the linear fit to determined Lamb dip positions vs. pressure with inverse squared fit uncertainty used as statistical weights.

under investigation and the minimal spectrum averaging time of 2 hours leads to the uncertainty below 3 Hz. Pressure is determined based on Doppler-limited measurements of transitions under investigation in low-power conditions, i.e. typically with intra-cavity power reduced by an order of magnitude or more compared to Lamb dip measurements, which corresponds to negligible saturation. Taking into account uncertainty of HITRAN [31] line intensities [27,46,47] (between 1% and 2%) and fit uncertainty (up to 4%), the pressure uncertainty contributes to relative uncertainty of the pressure shift at 4.5% level and the contribution to the uncertainty of the R7 transition frequency is nearly 0.17 kHz. The power shift that may be induced by the AC Stark effect has been verified by measurement of the Lamb dip position at intra-cavity power levels between 20 W and 150 W, and no Lamb dip position power dependence has been observed. The estimated uncertainty of the transition frequency caused by this effect is approximately 0.13 kHz, whereas in the case of the collisional shift coefficient it corresponds to relative uncertainty of 3.2%. Other sources of the transition frequency uncertainty arise from Lorentzian models of the Lamb dip shape and the cavity mode shape, and the stability of the beat-note frequency between the probe beam and the OFC which is mainly related to the stability of the optical cavity. These three affect the transition frequency determination at 0.1 kHz level, whereas only the dip shape model significantly affects the pressure shift coefficient determination. The second order Doppler effect leads to the transition frequency decrease of 0.28 kHz and its uncertainty is negligible. The recoil effect in the saturation regime leads to symmetric transition splitting of 5.81 kHz [48]. This is below our experimental resolution and effectively leads to negligible Lamb dip broadening.

The comparison of our results with the available literature data is shown in Table 1. R7 transition frequency agrees with the result of Wang et al. [43]. On the other hand, our transition frequency for the R10 line is higher by 2.6 kHz from the value by Wang et al. [39,42,43], which is 4 times the combined standard uncertainty. The transition frequencies are in agreement with values arising from the Doppler-limited measurement by Mondelain et al. [44] and Picqué et al. [45], however these values have uncertainties higher by three orders of magnitude than ours.

Optics EXPRESS

Table 2. Uncertainty budget for transition frequency and pressure shift coefficient for the R7 transition.

standard uncertainty	ν_0 (kHz)	Δ/p (kHz/Pa)
type A	0.257	0.322
contributions to type B:		
frequency reference accuracy	<0.003	<0.001
pressure determination	0.168	0.047
power shift	0.131	0.033
dip shape	0.1	0.025
cavity mode shape	0.1	<0.001
beat-note frequency stability	0.1	<0.001
2^{nd} order Doppler effect	<0.001	–
total standard uncertainty	0.38	0.33

We determine the collisional shift of transitions under investigation which was not observed by Wang et al. [39,42,43]. Our values are 40% lower than those by Picqué et al. [45].

One of reasons for the difference between collisional shift coefficients observed in Doppler-limited and saturation spectroscopy may arise from the relation between elastic and inelastic scattering [49,50]. Both the nonlinear pressure shift [51] and broadening [52] have already been observed in the saturation regime. Another reason may arise from the speed-dependent effects [53]. In the Lamb dip and Doppler-limited spectroscopy, the determined collisional shift coefficient value is differently averaged over the distribution of molecular velocities. In the first case, the molecular velocity in a direction parallel to the probe beam equals zero, whereas in the second one the Maxwellian distribution of velocities is averaged in all three dimensions.

4. Conclusions

In the article we introduce for the first time the CMDS and CMWS techniques to measurements in the saturation regime. We determine the most accurate transition frequencies for investigated CO lines from the second overtone, namely R7 and R10. We show that similarly as in the Doppler regime, CMDS leads to more accurate results than CRDS and CMWS. Even though the applied cavity mode shape model is significantly simplified, the determined Lamb dip position in CMDS is insensitive to the mode shape fitting frequency range and leads to the total uncertainty of unperturbed line position below 0.5 kHz. Compared to CMDS results, line positions retrieved from CRDS and CMWS are between 1.9 and 3.2 kHz higher, whereas collisional shift coefficients are up to 120% different. This is due to the systematic errors associated with saturated ring-down and mode transmission signal shapes. These differences might be significantly larger, depending on saturation level and chosen fitting approach. The advantage of the superb accuracy of the CMDS technique is strongly confirmed by the two measurement series performed two years apart from each other with different OFCs. Also, in contrast to available literature data from the saturation regime, we observe the Lamb dip collisional shift which points to the need for further study of its mechanism, including neglected here fundamental effects of speed dependence and interplay of elastic and inelastic scattering.

The presented technique can be implemented for stable molecules of fundamental interest such as HD, CO_2 and others for any lines that can be saturated with laser power available in the experiment. Due to the extended dynamic range compared to widely used CRDS, CMDS can be applied for transitions requiring higher saturating power.

Funding. Narodowe Centrum Nauki (2015/18/E/ST2/00585, 2016/23/B/ST2/00730, 2017/26/D/ST2/00371, 2018/30/E/ST2/00864, 2019/35/B/ST2/01118).

Optics EXPRESS

Acknowledgments. The research is part of the program of the National Laboratory FAMO in Torun, Poland, supported by the subsidy of the Ministry of Science and Higher Education.

Disclosures. The authors declare no conflicts of interest.

Data availability. Data underlying the results presented in this paper are not publicly available at this time but may be obtained from the authors upon reasonable request.

References

1. M. S. Safronova, D. Budker, D. DeMille, D. F. J. Kimball, A. Derevianko, and C. W. Clark, "Search for new physics with atoms and molecules," Rev. Mod. Phys. **90**(2), 025008 (2018).
2. N. R. Hutzler, "Polyatomic molecules as quantum sensors for fundamental physics," Quantum Sci. Technol. **5**(4), 044011 (2020).
3. E. J. Salumbides, J. C. J. Koelemeij, J. Komasa, K. Pachucki, K. S. E. Eikema, and W. Ubachs, "Bounds on fifth forces from precision measurements on molecules," Phys. Rev. D **87**(11), 112008 (2013).
4. J. Komasa, K. Piszczatowski, G. Łach, M. Przybytek, B. Jeziorski, and K. Pachucki, "Quantum electrodynamics effects in rovibrational spectra of molecular hydrogen," J. Chem. Theory Comput. **7**(10), 3105–3115 (2011).
5. F. M. J. Cozijn, P. Dupré, E. J. Salumbides, K. S. E. Eikema, and W. Ubachs, "Sub-Doppler frequency metrology in HD for tests of fundamental physics," Phys. Rev. Lett. **120**(15), 153002 (2018).
6. V. A. Dzuba, V. V. Flambaum, and J. K. Webb, "Space-time variation of physical constants and relativistic corrections in atoms," Phys. Rev. Lett. **82**(5), 888–891 (1999).
7. J. Biesheuvel, J.-P. Karr, L. Hilico, K. S. E. Eikema, W. Ubachs, and J. C. J. Koelemeij, "Probing QED and fundamental constants through laser spectroscopy of vibrational transitions in HD^+," Nat. Commun. **7**(1), 10385 (2016).
8. ACME Collaboration, V. Andreev, D. G. Ang, D. DeMille, J. M. Doyle, G. Gabrielse, J. Haefner, N. R. Hutzler, Z. Lasner, C. Meisenhelder, B. R. O'Leary, C. D. Panda, A. D. West, E. P. West, and X. Wu, "Improved limit on the electric dipole moment of the electron," Nature **562**(7727), 355–360 (2018).
9. J. J. Hudson, D. M. Kara, I. J. Smallman, B. E. Sauer, M. R. Tarbutt, and E. A. Hinds, "Improved measurement of the shape of the electron," Nature **473**(7348), 493–496 (2011).
10. M. Borkowski, A. A. Buchachenko, R. Ciuryło, P. S. Julienne, H. Yamada, Y. Kikuchi, Y. Takasu, and Y. Takahashi, "Weakly bound molecules as sensors of new gravitylike forces," Sci. Rep. **9**(1), 14807 (2019).
11. A. Derevianko and M. Pospelov, "Hunting for topological dark matter with atomic clocks," Nat. Phys. **10**(12), 933–936 (2014).
12. P. Wcisło, P. Morzyński, M. Bober, A. Cygan, D. Lisak, R. Ciuryło, and M. Zawada, "Experimental constraint on dark matter detection with optical atomic clocks," Nat. Astron. **1**(1), 0009 (2017).
13. F. Riehle, P. Gill, F. Arias, and L. Robertsson, "The CIPM list of recommended frequency standard values: guidelines and procedures," Metrologia **55**(2), 188–200 (2018).
14. G.-W. Truong, D. A. Long, A. Cygan, D. Lisak, R. D. van Zee, and J. T. Hodges, "Comb-linked, cavity ring-down spectroscopy for measurements of molecular transition frequencies at the kHz-level," J. Chem. Phys. **138**(9), 094201 (2013).
15. R. Gotti, D. Gatti, P. Masłowski, M. Lamperti, M. Belmonte, P. Laporta, and M. Marangoni, "Conjugating precision and acquisition time in a Doppler broadening regime by interleaved frequency-agile rapid-scanning cavity ring-down spectroscopy," J. Chem. Phys. **147**(13), 134201 (2017).
16. K. Bielska, S. Wójtewicz, P. Morzyński, P. Ablewski, A. Cygan, M. Bober, J. Domysławska, M. Zawada, R. Ciuryło, P. Masłowski, and D. Lisak, "Absolute frequency determination of molecular transition in the Doppler regime at kHz level of accuracy," J. Quant. Spectrosc. Radiat. Transfer **201**, 156–160 (2017).
17. Z. D. Reed, D. A. Long, H. Fleurbaey, and J. T. Hodges, "SI-traceable molecular transition frequency measurements at the 10^{-12} relative uncertainty level," Optica **7**(9), 1209–1220 (2020).
18. G. Giusfredi, S. Bartalini, S. Borri, P. Cancio, I. Galli, D. Mazzotti, and P. De Natale, "Saturated-absorption cavity ring-down spectroscopy," Phys. Rev. Lett. **104**(11), 110801 (2010).
19. M. de Labachelerie, K. Nakagawa, and M. Ohtsu, "Ultranarrow $^{13}C_2H_2$ saturated-absorption lines at 15 μm," Opt. Lett. **19**(11), 840–842 (1994).
20. D. Romanini, P. Dupré, and R. Jost, "Non-linear effects by continuous wave cavity ringdown spectroscopy in jet-cooled NO_2," Vib. Spectrosc. **19**(1), 93–106 (1999).
21. C. R. Bucher, K. K. Lehmann, D. F. Plusquellic, and G. T. Fraser, "Doppler-free nonlinear absorption in ethylene by use of continuous-wave cavity ringdown spectroscopy," Appl. Opt. **39**(18), 3154–3164 (2000).
22. J. Ye, L.-S. Ma, and J. L. Hall, "Sub-Doppler optical frequency reference at 1.064 μm by means of ultrasensitive cavity-enhanced frequency modulation spectroscopy of a C_2HD overtone transition," Opt. Lett. **21**(13), 1000–1002 (1996).
23. O. Axner, W. Ma, and A. Foltynowicz, "Sub-Doppler dispersion and noise-immune cavity-enhanced optical heterodyne molecular spectroscopy revised," J. Opt. Soc. Am. B **25**(7), 1166–1177 (2008).
24. A. Cygan, P. Wcisło, S. Wójtewicz, P. Masłowski, J. T. Hodges, R. Ciuryło, and D. Lisak, "One-dimensional frequency-based spectroscopy," Opt. Express **23**(11), 14472–14486 (2015).

Optics EXPRESS

25. A. Cygan, D. Lisak, P. Morzyński, M. Bober, M. Zawada, E. Pazderski, and R. Ciuryło, "Cavity mode-width spectroscopy with widely tunable ultra narrow laser," Opt. Express **21**(24), 29744–29754 (2013).
26. D. A. Long, G. W. Truong, R. D. van Zee, D. F. Plusquellic, and J. T. Hodges, "Frequency-agile, rapid scanning spectroscopy: Absorption sensitivity of 2×10^{-12} cm^{-1} Hz$^{-1/2}$ with a tunable diode laser," Appl. Phys. B: Lasers Opt. **114**(4), 489–495 (2014).
27. A. Cygan, P. Wcisło, S. Wójtewicz, G. Kowzan, M. Zaborowski, D. Charczun, K. Bielska, R. S. Trawiński, R. Ciuryło, P. Masłowski, and D. Lisak, "High-accuracy and wide dynamic range frequency-based dispersion spectroscopy in an optical cavity," Opt. Express **27**(15), 21810–21821 (2019).
28. S. Wójtewicz, D. Lisak, A. Cygan, J. Domysławska, R. S. Trawiński, and R. Ciuryło, "Line-shape study of self-broadened O_2 transitions measured by Pound-Drever-Hall-locked frequency-stabilized cavity ring-down spectroscopy," Phys. Rev. A **84**(3), 032511 (2011).
29. A. J. Fleisher, E. M. Adkins, Z. D. Reed, H. Yi, D. A. Long, H. M. Fleurbaey, and J. T. Hodges, "Twenty-five-fold reduction in measurement uncertainty for a molecular line intensity," Phys. Rev. Lett. **123**(4), 043001 (2019).
30. J. T. Hodges, H. P. Layer, W. W. Miller, and G. E. Scace, "Frequency-stabilized single-mode cavity ring-down apparatus for high-resolution absorption spectroscopy," Rev. Sci. Instrum. **75**(4), 849–863 (2004).
31. I. E. Gordon, L. S. Rothman, C. Hill, R. V. Kochanov, Y. Tan, P. F. Bernath, M. Birk, V. Boudon, A. Campargue, K. V. Chance, B. J. Drouin, J.-M. Flaud, R. R. Gamache, J. T. Hodges, D. Jacquemart, V. I. Perevalov, A. Perrin, K. P. Shine, M.-A. H. Smith, J. Tennyson, G. C. Toon, H. Tran, V. G. Tyuterev, A. Barbe, A. G. Császár, V. M. Devi, T. Furtenbacher, J. J. Harrison, J.-M. Hartmann, A. Jolly, T. J. Johnson, T. Karman, I. Kleiner, A. A. Kyuberis, J. Loos, O. M. Lyulin, S. T. Massie, S. N. Mikhailenko, N. Moazzen-Ahmadi, H. S. P. Müller, O. V. Naumenko, A. V. Nikitin, O. L. Polyansky, M. Rey, M. Rotger, S. W. Sharpe, K. Sung, E. Starikova, S. A. Tashkun, J. V. Auwera, G. Wagner, J. Wilzewski, P. Wcisło, S. Yu, and E. J. Zak, "The HITRAN2016 molecular spectroscopic database," J. Quant. Spectrosc. Radiat. Transf. **203**, 3–69 (2017).
32. G.-W. Truong, K. O. Douglass, S. E. Maxwell, R. D. van Zee, D. F. Plusquellic, J. T. Hodges, and D. A. Long, "Frequency-agile, rapid scanning spectroscopy," Nat. Photonics **7**(7), 532–534 (2013).
33. M. Zaborowski, M. Słowiński, K. Stankiewicz, F. Thibault, A. Cygan, H. Jóźwiak, G. Kowzan, P. Masłowski, A. Nishiyama, N. Stolarczyk, S. Wójtewicz, R. Ciuryło, D. Lisak, and P. Wcisło, "Ultrahigh finesse cavity-enhanced spectroscopy for accurate tests of quantum electrodynamics for molecules," Opt. Lett. **45**(7), 1603–1606 (2020).
34. R. W. P. Drever, J. L. Hall, F. V. Kowalski, J. Hough, G. M. Ford, A. J. Munley, and H. Ward, "Laser phase and frequency stabilization using an optical resonator," Appl. Phys. B **31**(2), 97–105 (1983).
35. C. Salomon, D. Hils, and J. L. Hall, "Laser stabilization at the millihertz level," J. Opt. Soc. Am. B **5**(8), 1576–1587 (1988).
36. A. Cygan, S. Wójtewicz, G. Kowzan, M. Zaborowski, P. Wcisło, J. Nawrocki, P. Krehlik, L. Śliwczyński, M. Lipiński, P. Masłowski, R. Ciuryło, and D. Lisak, "Absolute molecular transition frequencies measured by three cavity-enhanced spectroscopy techniques," J. Chem. Phys. **144**(21), 214202 (2016).
37. J. Lee and J. Hahn, "Theoretical analysis on the dynamic absorption saturation in pulsed cavity ringdown spectroscopy," Appl. Phys. B **79**(5), 653–662 (2004).
38. J. Burkart, T. Sala, D. Romanini, M. Marangoni, A. Campargue, and S. Kassi, "Communication: Saturated CO_2 absorption near 1.6 μm for kilohertz-accuracy transition frequencies," J. Chem. Phys. **142**(19), 191103 (2015).
39. J. Wang, Y. R. Sun, L. G. Tao, A. W. Liu, and S. M. Hu, "Communication: Molecular near-infrared transitions determined with sub-kHz accuracy," J. Chem. Phys. **147**(9), 091103 (2017).
40. W. Ma, A. Foltynowicz, and O. Axner, "Theoretical description of Doppler-broadened noise-immune cavity-enhanced optical heterodyne molecular spectroscopy under optically saturated conditions," J. Opt. Soc. Am. B **25**(7), 1144–1155 (2008).
41. K. Bielska, J. Domysławska, S. Wójtewicz, A. Balashov, M. Słowiński, M. Piwiński, A. Cygan, R. Ciuryło, and D. Lisak, "Simultaneous observation of speed dependence and Dicke narrowing for self-perturbed P-branch lines of O_2 B band," J. Quant. Spectrosc. Radiat. Transf. **276**, 107927 (2021).
42. J. Wang, Y. R. Sun, L. G. Tao, A. W. Liu, and S. M. Hu, "Erratum: "Communication: Molecular near-infrared transitions determined with sub-kHz accuracy" [J. Chem. Phys. 147, 091103 (2017)]," The J. Chem. Phys. **148**(2), 029902 (2018).
43. J. Wang, C.-L. Hu, A.-W. Liu, Y. Sun, Y. Tan, and S.-M. Hu, "Saturated absorption spectroscopy near 1.57 μm and revised rotational line list of $^{12}C^{16}O$," J. Quant. Spectrosc. Radiat. Transf. **270**, 107717 (2021).
44. D. Mondelain, T. Sala, S. Kassi, D. Romanini, M. Marangoni, and A. Campargue, "Broadband and highly sensitive comb-assisted cavity ring down spectroscopy of CO near 1.57μm with sub-MHz frequency accuracy," J. Quant. Spectrosc. Radiat. Transf. **154**, 35–43 (2015).
45. N. Picqué and G. Guelachvili, "Absolute wavenumbers and self-induced pressure lineshift coefficients for the 3-0 vibration–rotation band of $^{12}C^{16}O$," J. Mol. Spectrosc. **185**(2), 244–248 (1997).
46. G. Li, I. E. Gordon, L. S. Rothman, Y. Tan, S. M. Hu, S. Kassi, A. Campargue, and E. S. Medvedev, "Rovibrational line lists for nine isotopologues of the CO molecule in the $X^1\Sigma^+$ ground electronic state," Astrophys. J., Suppl. Ser. **216**(1), 15 (2015).
47. Y. G. Borkov, A. M. Solodov, A. A. Solodov, T. M. Petrova, E. V. Karlovets, and V. I. Perevalov, "Fourier transform CO spectra near 1.6 μm," J. Quant. Spectrosc. Radiat. Transf. **253**, 107064 (2020).

Optics EXPRESS

48. J. L. Hall, C. J. Bordé, and K. Uehara, "Direct optical resolution of the recoil effect using saturated absorption spectroscopy," Phys. Rev. Lett. **37**(20), 1339–1342 (1976).
49. S. N. Bagaev, E. V. Baklanov, and V. P. Chebotaev, "Anomalous decrease of the shift of the center of the Lamb dip in low-pressure molecular gases," Soviet Journal of Experimental and Theoretical Physics Letters **16**(6), 243–246 (1972).
50. V. A. Alekseev, T. L. Andreeva, and I. I. Sobel'man, "Contribution to the theory of nonlinear power resonances in gas lasers," JETP **37**(3), 413–417 (1973).
51. S. N. Bagaev and V. P. Chebotaev, "Laser frequency standards," Sov. Phys. Uspekhi **29**(1), 82–103 (1986).
52. T. W. Meyer, C. K. Rhodes, and H. A. Haus, "High-resolution line broadening and collisional studies in CO_2 using nonlinear spectroscopic techniques," Phys. Rev. A **12**(5), 1993–2008 (1975).
53. S. Wójtewicz, A. Cygan, K. Kropidłowska, M. Marangoni, P. Masłowski, D. Lisak, and R. Ciuryło, "Speed-dependent effects in Doppler-free saturation spectra," J. Mol. Spectrosc. **351**, 21–28 (2018).

158.75.105.70 {2036.03.05 04:30:15}